A novel hybrid robot and its processes for precision polishing of freeform surfaces

Peng Xu [a, b], Chi Fai Cheung [a*], Chunjin Wang [a], Chenyang Zhao [a, b]

[a] State Key Laboratory of Ultra-precision Machining Technology, Department of Industrial and Systems Engineering, The Hong Kong Polytechnic University, Hung Hom, Kowloon, Hong Kong

[b] School of Mechanical Engineering and Automation, Harbin Institute of Technology, Shenzhen 518055, China

* Corresponding author

E-mail address: benny.chenung@polyu.edu.hk (C.F. Cheung)

Abstract: Freeform surfaces have important applications in various industrial fields. However, achieving a high level surface finish on freeform surfaces using polishing is always a challenging task. Hybrid robots are promising alternatives to conventional computer numerical control (CNC) machines and industrial robots for ultra-precision machining. Herein, we present a novel custom-built hybrid robot for freeform polishing. After the laboratory prototype was successfully developed, its automation for a specific freeform surface was a major obstacle preventing its application. This critical issue was addressed by presenting a process to deal with tedious robot programming. Random tool path planning was performed in the task space, and hybrid robot motion planning was conducted in the joint space. By integrating the process flows, a robot programming toolkit was developed to directly output the control program for a specific robot controller. An illustrative example with a freeform surface is provided to verify the functionality of the developed hybrid robot and the proposed control processes, and the corresponding experimental results verify their effectiveness.

Keywords: Hybrid robot; precision polishing; freeform surface; random path; ultra-precision machining

1 Introduction

With the rapid advancement of astronomy, precision molds, and advanced optical instruments, freeform surfaces have been widely applied to improve the design and enhance the functional characteristics of devices. Precision polishing has long been applied in high-quality freeform manufacturing. However, the conventionally used manual processes for freeform surface polishing were complex and inaccurate, computer-controlled polishing techniques have been developed to automate this process. Such processes usually use conventional computer numerical control (CNC) machines [1-5] and industrial robots [6-10] with specially designed tooling systems. For computer-controlled polishing, the control codes must be prepared according to the surface geometry and pre-selected process parameters [11]; this usually requires professional knowledge from the operators. Recently, computers have been widely used to assist in this operation. At present, computer-aided manufacturing (CAM) software, such as MasterCAM, UG NX, and CATIA for CNC machines, or Robotmaster and RobotStudio for industrial robots, can provide complete processes for tool-path generation, postprocessing, simulation, and control code generation. These technologies significantly reduce the mistakes made by operators and improve the quality of control codes.

According to the structural topology, conventional CNC machines and industrial robots are mainly developed based on serial manipulators, where actuators are connected one-by-one in series. To ensure stiffness, bulky structures are often required, resulting in a large moving mass and a low strength-to-weight ratio. Parallel manipulators can combat this issue by using fixed actuators and low moving masses. However, parallel manipulators also suffer several disadvantages, such as a small and irregular workspace, limited orientational motion range, and highly inconsistent dexterity within the workspace. Therefore, hybrid manipulators have attracted increasing attention in various industrial fields, especially in ultra-precision machining. By combining serial and parallel manipulators, hybrid manipulators can boast of advantages of both parts. Thus far, compared with the milling process, only a few attempts have been made to develop robots based on hybrid manipulators for ultra-precision polishing [12-14]. Because of their inherent complexities, generation of control programs for hybrid robots to conduct freeform polishing is a laborious and time-consuming task, the automation of which is still in progress.

In the milling process with hybrid robots, the tool paths are practically converted from the

cutter location (CL) data [15] or interpreted from the G-code [16] generated by CAM software. However, the process of material removal during polishing is fundamentally different from that during milling. Therefore, tool-path generation has attracted significant attention for the polishing process. Generally, tool-path generation in the workpiece frame for a given part is called preprocessing. Cao et al. [17] used the raster tool path to investigate surface generation mechanisms in the polishing process. The results indicated that the surface texture exhibited a periodic gouge because of the superposition effects of adjacent paths. Although polishing results can be further enhanced by optimizing the side step and forward step [18], various tool paths using random curves have been presented in recent years. To achieve overall uniformity and directional isotropy of the polished surfaces, Dunn and Walker [19] proposed a tool path that could be spread in six directions. Wang et al. [20] proposed a maze tool path and confirmed that it could avoid the appearance of periodical structures. Based on circular elements, a random tool path was also proposed by Takizawa and Beaucamp [21] to suppress repetitive patterns and reduce surface waviness. Dong and Nai [22] proposed an algorithm to generate random tool paths that could fill different areas. Tam and Cheng [23] compared the effect of four tool paths on material removal and showed that the direction of the tool path should be well distributed and balanced. The above discussion indicates that most previous studies have mainly focused on tool-path generation on flat surfaces in the XY plane. More in-depth investigation of random path generation on freeform surfaces is required.

The tool paths generated in the workpiece frame cannot be directly used for machinery control. To achieve the desired polishing action using the tool on the workpiece, control codes should be generated that can be accepted by a specific robot controller. This process is called postprocessing. However, the previous studies on postprocessor developed have mostly focused on serial-type CNC machines. Currently, CAM software can provide postprocessors for the most widely used machines. Because postprocessing highly depends on structural configurations, a specially designed postprocessor of a hybrid robot is essential for practical applications. Lin et al. [24] introduced a robotic polishing system and developed a postprocessor for complex surface polishing that used a tool-path generator based on CL data. Chen et al. [25] investigated the postprocessing strategy of a five degree-of-freedom (DOF) hybrid machine that could directly generate the control code. Lai et al. [15] presented a modular method to construct a postprocessor system for a hybrid robot. Wang

et al. [16] investigated a postprocessing method of a three-DOF parallel tool head for five-axis milling. Because of various structural configurations, studies on dedicated postprocessor development for the hybrid robots with multiple parallel limbs and non-orthogonal axes should be conducted individually.

Overall, although CAM has significantly advanced, it cannot be directly applied to hybrid robots for polishing freeform surfaces because of the incapable tool-path generator and unavailable postprocessors. Numerous studies have focused on these two topics. On one hand, some researchers individually studied tool-path generators on the flat surfaces, which were independent of the configurations of the robot. The tool path was then achieved using commercial machines or robots with their embedded postprocessors. On the other hand, some studies have investigated the postprocessing strategy of hybrid robots for prescribed tool paths. The design a tool path generator and preprocessors has been independent of each other. In response to the insufficiency of previous studies, we aim to design a feasible custom-built hybrid robot and present a complete process to achieve freeform polishing. By combining tool-path planning in the task space and actuator motion planning in the joint space, we developed a programming toolkit for the considered hybrid robot, which can automatically and directly output the appropriate control file format for the robotic controller without further editing.

The rest of the paper is organized as follows: following the introduction section, Section 2 describes the developed hybrid robot and its related kinematic performances. Section 3 presents the algorithm of the random tool-path generator on freeform surfaces and the robot postprocessing algorithm to convert the tool path into the control code. Section 4 demonstrates the application of the hybrid robot on a freeform surface, and the conclusions are provided in Section 5.

2 Hybrid robot description

Fig. 1 shows the design of the polishing machine. It essentially comprises a six-DOF hybrid robot, control console, control cabinet, and coolant/slurry tank. The hybrid robot comprises a spatial parallel robot with three translations and one rotation for positioning the workpiece and an A/C-type serial robot to orient the tool. The spatial parallel robot features three symmetrically arranged 3-$\underline{P}(SS)^2$ limbs and a functional extension $\underline{R}$UPUR limb located in the middle. Here, P, S, R, and U

denote the prismatic joint, spherical joint, revolute joint, and universal joint, respectively, while the underlined P and R represent the actuated prismatic joint and actuated revolute joint, respectively. The active prismatic joints are driven by servo motors with lead screws, and the active revolute joints are driven by servo motors with reducers. The hybrid robot is controlled by the Power PMAC controller from Delta Tau Data Systems, Inc (Los Angeles, CA, USA). Based on this design, a laboratory prototype of the hybrid robot was built, as shown in Fig. 2. Currently, the prototype of the hybrid robot is used in The Hong Kong Polytechnic University, and the polishing process parameters are pre-determined off-line. The development of the prototype is on-going to provide more functions.

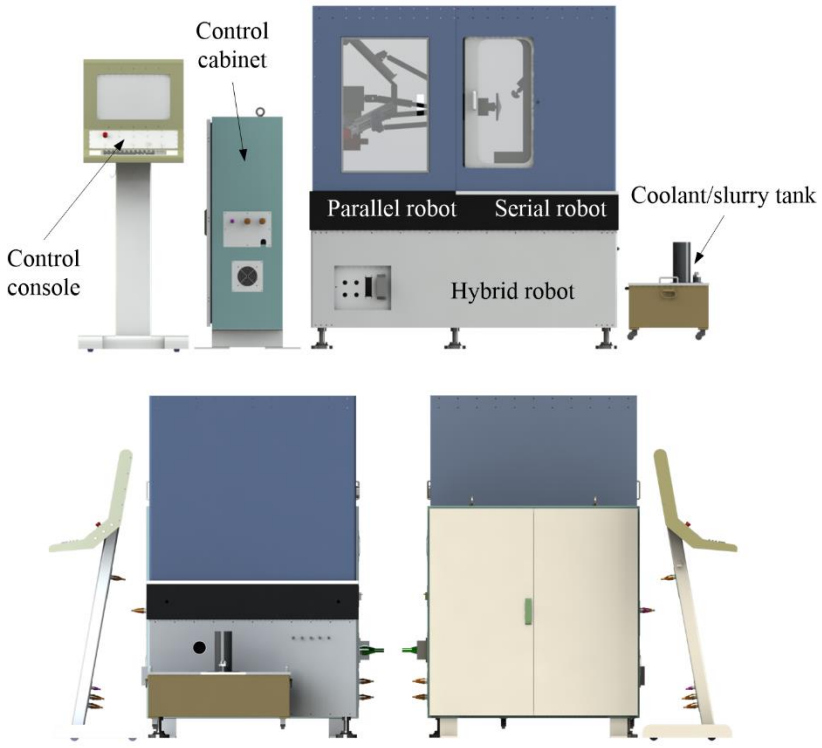

(a)

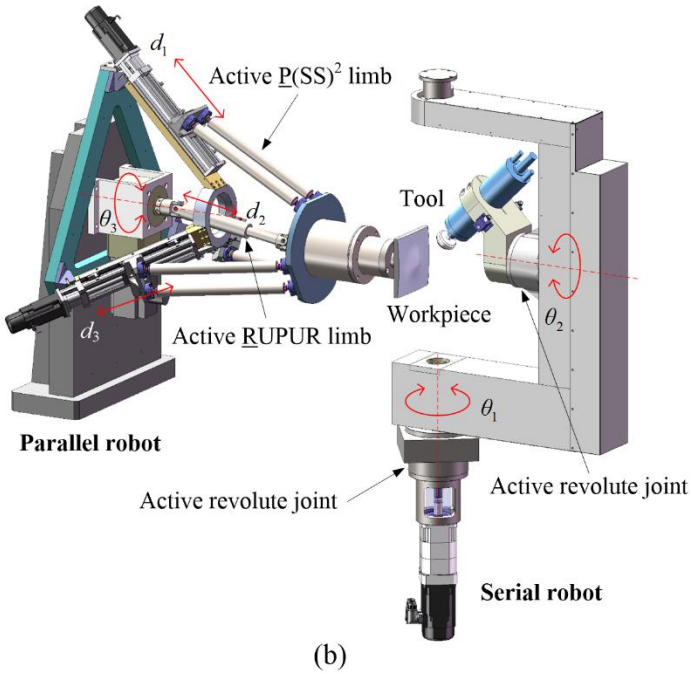

(b)

Fig. 1 Polishing machine with the hybrid robot: (a) layout of the polishing machine; (b) 3D view of the hybrid robot.

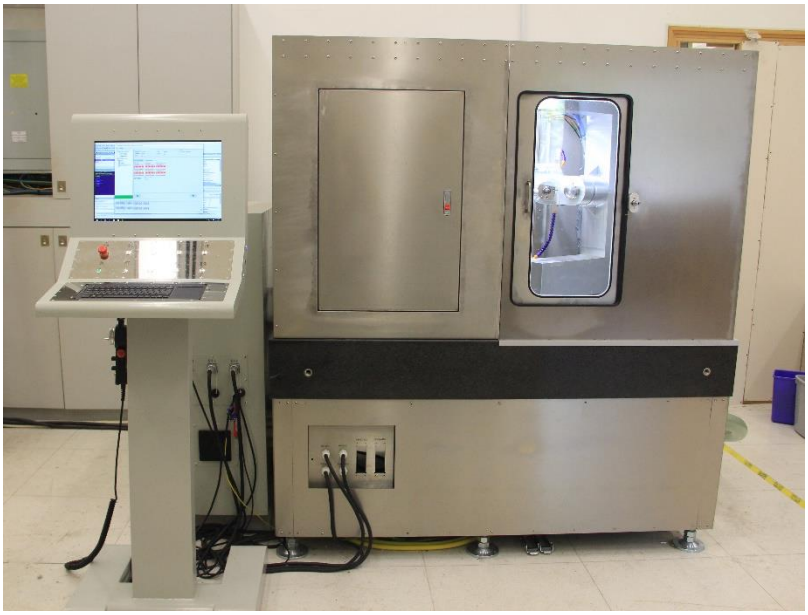

Fig. 2 Laboratory prototype of the polishing machine with the hybrid robot.

Fig. 3 shows the geometric parameters of the hybrid robot. For the convenience of analysis, some denotations are defined here. The three actuated limbs in the parallel robot are denoted as limb 1, 2, and 3, and the middle limb plus the clamp are denoted as limb 4. A_i (i = 1, 2, 3) represents the intersections of the prismatic joint axes of limb i with the normal plane, in which all three zero positions in the prismatic joints are placed. C_i and D_i denote the centers of the two spherical joints connected to the slider and the moving platform in limb i. In addition, the base frame $\{O_b\}$, workpiece frame $\{O_w\}$, and tool frame $\{O_t\}$ are established.

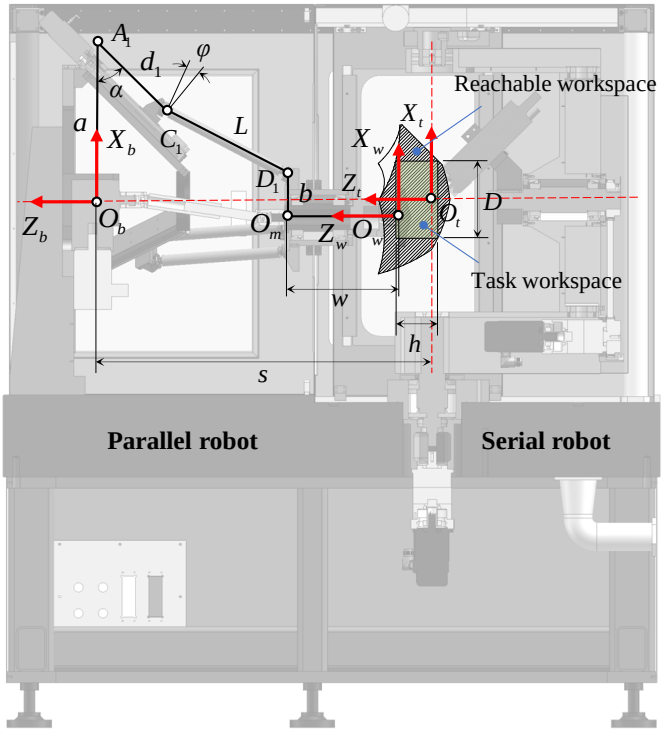

Fig. 3 Geometric parameters and cross-sectional view of the workspace of the hybrid robot.

Table 1 lists the dimensional parameters of the parallel robot, where θ_{smax} is the maximum motion range of the passive spherical joint; d_{min} and d_{max} are the motion ranges of the active prismatic joint. The other symbols are introduced in Fig. 3. As stated in the introduction, the disadvantages of parallel robots include a complex workspace and highly inconsistent dexterity. Hence, Fig. 4 graphically illustrates the 3D workspace of the parallel robot. To improve the reachable workspace as much as possible, a maximum inscribed cylinder is defined as the task workspace. It is located within the reachable workspace, and the ratio of diameter D to height h is 2 to 1. The singular configurations of the robot lead to controllability loss and stiffness degradation, which can be evaluated using various dexterity indices. One of the dexterity indices is defined as the reciprocal of the condition number of the Jacobian matrix [26]. Fig. 5 shows the distributions of the dexterity indices of the different layers of the workspace, where 0 indicates that the parallel robot is in a singular configuration. The parallel robot clearly has no singularity position in the prescribed task workspace where the actual polishing operations are performed.

Table 1 Geometric parameters of the hybrid robot

Parameters	Values	Units	Parameters	Values	Units
a	300.63	mm	d_{min}	-30	mm
b	122.38	mm	d_{max}	170	mm
L	370	mm	θ_{smax}	30	°
w	294.37	mm	s	971.42	mm
α	45	°	φ	17	°
D	222.8	mm	h	111.4	mm

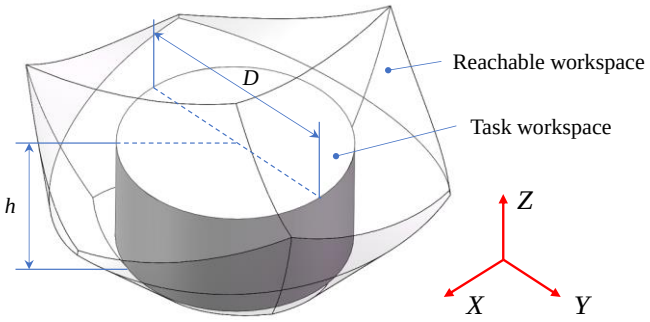

Fig. 4 Reachable workspace and task workspace of the parallel robot.

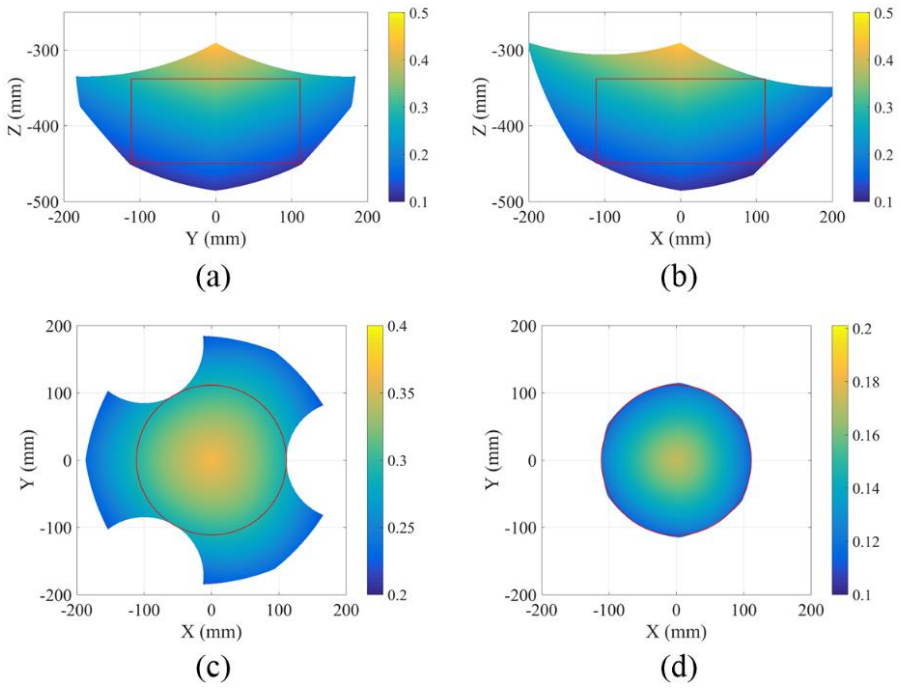

Fig. 5. Dexterity distribution of the parallel robot within the workspace: (a) $X = 0$ cross-section, (b) $Y = 0$ cross-section, (c) top cross-section, and (d) bottom cross-section.

3 Motion planning for freeform polishing

Robot motion planning should be conducted in both the task space and the joint space for the hybrid robot. This section presents a tool-path generator to plan the motion of the tool in the task space and a robot postprocessor to transform the motion into the joint space. A toolkit for integrating these processes, which can minimize programming effort, is developed.

3.1 Circular random curve

We assumed that the different conditions of incoming materials are considered and evaluated before polishing. Only the required area was chosen for tool-path planning. In addition to the widely used raster and spiral tool paths, various studies have aimed to improve the polishing quality using the fractal-based tool paths and their variants. Fractal-based tool paths have been investigated in various fields, such as polishing [23], sheet forming [27], and additive manufacturing [28]. As discussed previously, a reasonable tool path for the polishing process should fulfill several requirements, including space-filling, isotropy, and motion controllability. Space-filling requires the refining tool paths to be able to pass through each point and uniformly cover the entire surface. Isotropy means that the tool paths should have good randomization, which is multidirectional and uncrossed. For motion controllability, the shape of tool paths should to be as simple as possible with no sharp turns while changing directions.

The Hilbert curve [2], which is an attractive candidate among the fractal-based paths, was adopted in this study. It is a continuous path that can visit every point uniformly as the number of iterations increases. However, the minimum elements of the standard Hilbert curve are straight lines, and the elements are mutually orthogonal at turns. The multidirectional characteristic leads to extensive changes in directions. When the feed rate is high, severe vibrations may occur, thus affecting the surface quality and longevity of the machines. Therefore, the sharp angular transitions in the standard Hilbert curve are rounded by circle arcs. The generated standard Hilbert curves and the modified Hilbert curves rounded by circle arcs are illustrated in Fig. 6.

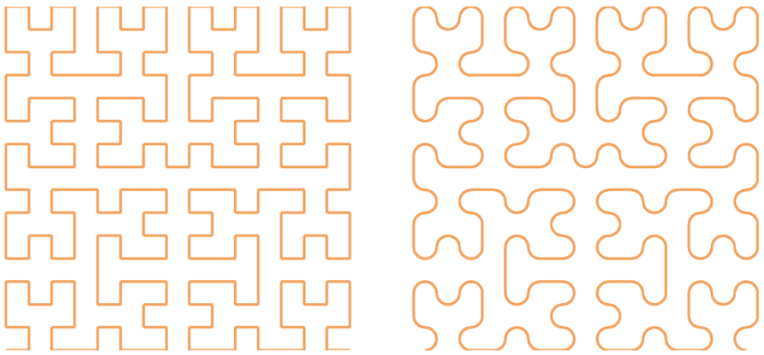

Fig. 6 Hilbert curve: (a) standard Hilbert curve, and (b) rounded Hilbert curve.

3.2 Tool-path generator

An accurate mathematical tool is required to describe freeform surfaces. In some prior studies, freeform surfaces were described using explicit formulas in the Euclidean space with the form $z = f(x, y)$ [29, 30]. For these surfaces, the tool path can be created on a freeform surface using the projection method. However, most freeform surfaces are defined in the parametric space and are based on control points specified in the Euclidean space, such as Bézier, B-spline, and non-uniform rational B-spline surface. For these surfaces, tool-path generation involves three steps [2]: path generation in the parametric space, path generation in the Euclidean space, and tool-axis orientation computation.

A Bézier surface is used here as an example to describe a freeform surface. Mathematically, a Bézier surface is constructed by two group of Bézier curves $B_{i,n}(u)$ and $B_{j,m}(v)$, which can be expressed as [31]

$$\boldsymbol{S}(u,v)=\sum_{i=0}^{n}\sum_{j=0}^{m}P_{ij}B_{i,n}(u)B_{j,m}(v),\quad 0\le u,\quad v\le 1 \tag{1}$$

where P_{ij} denotes the control points of $\boldsymbol{S}(u, v)$ with u and v being the parametric directions, and $B_{i,n}(t)$ is n-th degree Bernstein polynomials represented by

$$B_{i,n}(t)=\frac{n!}{i!(n-1)!}t^{i}(1-t)^{n-i},\ i=0, 1, \ldots, n \tag{2}$$

A parametric surface can be regarded as a mapping function from a point on the 2D parametric

space to a point in the 3D Euclidean space. The parameters u and v are defined in a plane area. Because the Hilbert curve is also defined in a plane area, one parameter that enables the construction of a curve needs to be specified as a function of the other parameter [32]. The mapping relationship is shown in Fig. 7. The Hilbert curve generated on the 2D plane is mapped into the parametric space of the freeform surface directly and then translated to the dwell point path on the corresponding freeform surface in the Euclidean space.

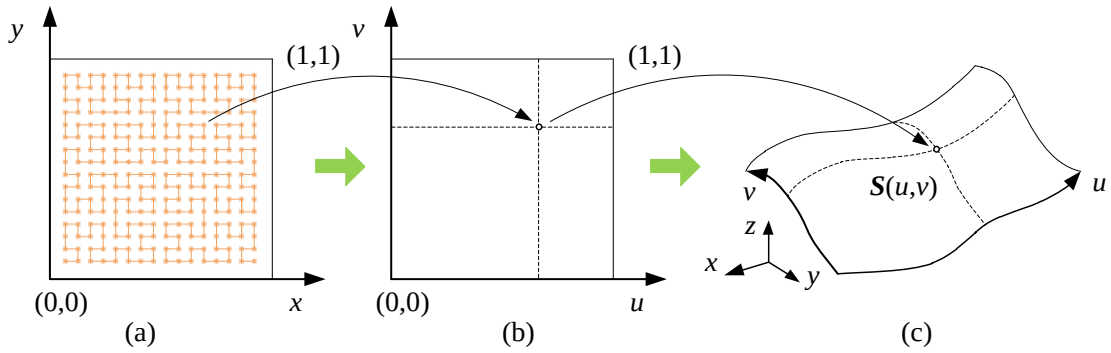

Fig. 7 Mapping relationship: (a) Hilbert curve, (b) parametric space, and (c) Euclidean space.

For the convenience of expression, Eq. (2) is organized into a matrix. The control points include m rows and n columns, and the expressions of $x(u, v)$, $y(u, v)$, and $z(u, v)$ on the Bézier surface become

$$\begin{cases} x(u,v)=\boldsymbol{B}_{m-1}^{\mathrm{T}}(u)\cdot\boldsymbol{P}_{mn}^{x}\cdot\boldsymbol{B}_{n-1}(v) \\ y(u,v)=\boldsymbol{B}_{m-1}^{\mathrm{T}}(u)\cdot\boldsymbol{P}_{mn}^{y}\cdot\boldsymbol{B}_{n-1}(v) \\ z(u,v)=\boldsymbol{B}_{m-1}^{\mathrm{T}}(u)\cdot\boldsymbol{P}_{mn}^{z}\cdot\boldsymbol{B}_{n-1}(v) \end{cases} \tag{3}$$

where $\boldsymbol{B}_{k-1}(\alpha)=[B_{k-1}^{0}(\alpha),B_{k-1}^{1}(\alpha),\cdots,B_{k-1}^{k-1}(\alpha)]^{\mathrm{T}}$, $\boldsymbol{P}_{mn}^{x}=\{P_{ij}^{x}\}$, $\boldsymbol{P}_{mn}^{y}=\{P_{ij}^{y}\}$, and $\boldsymbol{P}_{mn}^{z}=\{P_{ij}^{z}\}$.

Assuming that the Bézier surface is set within the range of $[X_s, X_e] \times [Y_s, Y_e]$, the following affine transformation can be used to transform the u-v domain to the x-y domain:

$$u=\frac{x-X_s}{X_e-X_s},\quad v=\frac{y-Y_s}{Y_e-Y_s} \tag{4}$$

The surface is evenly divided into $m \times n$ points. As a result, $P_{ij}^{x}=X_s+\frac{i-1}{m-1}(X_e-X_s)$ and

$P_{ij}^{y}=Y_s+\frac{j-1}{n-1}\left(Y_e-Y_s\right)$. The Bernstein polynomial is endowed with a binomial expansion $\sum_{i=0}^{n}B_n^i\left(\alpha\right)=1$. Then, the identical relation for $x(u, v)$ and $y(u, v)$ is

$$\begin{cases} x\left(\dfrac{x-X_s}{X_e-X_s},t\right)=x \\ y\left(t,\dfrac{y-Y_s}{Y_e-Y_s}\right)=y \end{cases} \tag{5}$$

Consequently, the freeform surface can be expressed as

$$z\left(x,y\right)=\boldsymbol{B}_{m-1}^{\mathrm{T}}\left(\frac{x-X_s}{X_e-X_s}\right)\cdot\boldsymbol{P}_{mn}^{z}\cdot\boldsymbol{B}_{n-1}\left(\frac{y-Y_s}{Y_e-Y_s}\right) \tag{6}$$

In addition, the normal vector can be calculated from [33], as follows:

$$\boldsymbol{n}_W=\frac{\boldsymbol{S}_u\times\boldsymbol{S}_v}{\left|\boldsymbol{S}_u\times\boldsymbol{S}_v\right|} \tag{7}$$

where $\boldsymbol{S}_u$ is the partial derivative of the surface with respect to the parameter u, and $\boldsymbol{S}_v$ is the partial derivative of the surface with respect to v. The direction of the normal is fixed by the convention that $\boldsymbol{S}_u$, $\boldsymbol{S}_v$, and $\boldsymbol{n}_w$ in this order form a right-handed system.

Once a parametric curve on a parametric space is given, any tool paths on the flat surfaces can be mapped onto the freeform surfaces. It should be noted that a curve in the parametric space is mapped to the Euclidean space in a nonlinear manner. When the curvature of a surface becomes significant, the ratio between the two spaces should be considered [32]. Nevertheless, this method can provide a uniform distribution of the tool path, which is good enough on slightly curved freeform surfaces [2].

Next, the path dwell points generated on the freeform surface must be converted into the motion of the tool center point (TCP). Fig. 8 shows the relationship between the surface dwell point and the TCP, where $\boldsymbol{n}_w$ is the unit vector of the local surface normal at each dwell point, $\boldsymbol{O}_t$ is the unit vector of the tool axis, $\boldsymbol{P}_c$ is the position of a surface dwell point, $\boldsymbol{P}_t$ is the position of a TCP, ρ is the incline angle between $\boldsymbol{n}_w$ and $\boldsymbol{O}_t$, ϕ is the attitude angle of $\boldsymbol{O}_t$ rotating about $\boldsymbol{n}_w$, R_b is the radius of the tool, and d is the tool offset.

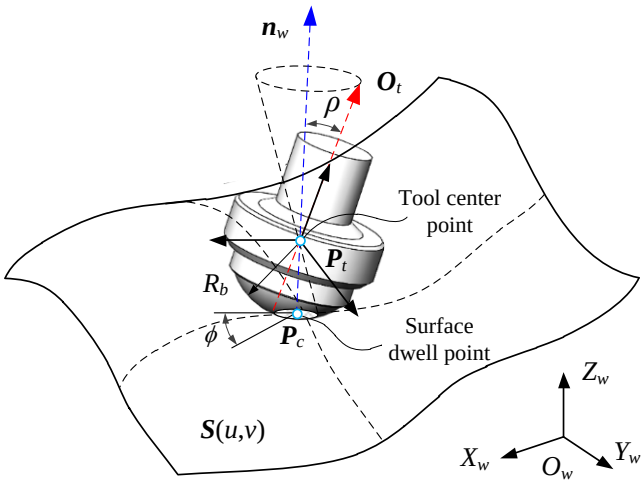

Fig. 8. Relationship between the surface dwell point and the TCP.

The position vector of TCP can be obtained by offsetting the surface dwell point along its normal direction:

$$\boldsymbol{P}_t = \boldsymbol{P}_c + \boldsymbol{n}_w\left(R_b - d\right) \tag{8}$$

A fixed angle ρ is desired to maintain a constant speed distribution on the surface. This means that the tool axis should lie on a cone of angle ρ around $\boldsymbol{n}_w$, and the attitude position on this cone is specified by ϕ. Then, the tool-axis vector can be expressed as

$$\boldsymbol{O}_t = \mathrm{Rot}\left(\boldsymbol{n}_w, \phi\right)\mathrm{Rot}\left(\boldsymbol{Y}_w, \rho\right)\boldsymbol{n}_w \tag{9}$$

where Rot denotes the corresponding rotational transformation matrix.

The combination of $\boldsymbol{P}_t$ and $\boldsymbol{O}_t$ denotes the tool location data, which are all described in the workpiece frame.

3.3 Robot postprocessor

After generating tool location data, the next step is to determine the set of joint variables and transform them into control codes of a specific robot controller through postprocessing. This transformation heavily relies on the modeling and properties of the hybrid robot.

As a function of the set of actuator inputs, the homogeneous transformation matrices (HTMs) of the workpiece frame with respect to the base frame $\boldsymbol{T}_{bw}$ and the tool frame with respect to the

base frame $\boldsymbol{T}_{bt}$ can be expressed as

$$\begin{aligned}\boldsymbol{T}_{bw}\left(d_1,d_2,d_3,\theta_3\right)&=\mathrm{Trans}\left(x,y,z\right)\mathrm{Rot}\left(z,\theta_3\right)\boldsymbol{T}_{bw}^{0},\\ \boldsymbol{T}_{bt}\left(\theta_1,\theta_2\right)&=\mathrm{Rot}\left(x,\theta_1\right)\mathrm{Rot}\left(y,\theta_2\right)\boldsymbol{T}_{bt}^{0}\end{aligned}\tag{10}$$

where d_i and θ_i, (i = 1, 2, 3) are the variables of actuated prismatic and revolute joints, as illustrated in Fig. 1, Trans denotes the corresponding translational transformation matrix, (x, y, z) represent the positions of the workpiece frame, which can be calculated from the forward kinematics of the parallel robot, and $\boldsymbol{T}_{bw}^{0}$ and $\boldsymbol{T}_{bt}^{0}$ denote the initial reference configuration of the workpiece frame and tool frame with respect to the base frame, respectively.

Consequently, the HTM of the tool frame relative to the workpiece frame is given by

$$\boldsymbol{T}_{wt}\left(d_1,d_2,d_3,\theta_1,\theta_2,\theta_3\right)=\left(\boldsymbol{T}_{bw}\right)^{-1}\boldsymbol{T}_{bt}\tag{11}$$

According to the structural parameters, the TCP position vector and tool-axis orientation vector relative to the tool frame are represented as $\boldsymbol{r}_t$ and $\boldsymbol{o}_t$, respectively. Then, the position and orientation vectors of the tool expressed in the base frame for a given set of actuator joint variables can be expressed as follows:

$$\begin{bmatrix}\boldsymbol{P}_t & \boldsymbol{O}_t\\ 1 & 0\end{bmatrix}=\boldsymbol{T}_{wt}\left(d_1,d_2,d_3,\theta_1,\theta_2,\theta_3\right)\begin{bmatrix}\boldsymbol{r}_t & \boldsymbol{o}_t\\ 1 & 0\end{bmatrix}\tag{12}$$

The kinematics model has been previously studied [34]. Once the tool location data are generated, the motion in the joint space can be calculated according to Eq. (12). In addition, the feed rate information must be assigned. Generally, the polishing process can be divided into two steps, i.e. pre-polishing and corrective polishing [35]. In particular, the pre-polishing step is conducted with a constant feed rate to remove the subsurface damage or decrease surface roughness. In contrast, corrective polishing can precisely correct the surface errors by converting the dwell time into the feed rate along the tool path. This means that every dwell point on the tool path should be assigned a different feed rate calculated from the error map. The precision of the tool path and the feed rate are two important factors on which polishing quality depends.

All this information should be formatted into the correct syntax such that the hybrid robot controller can recognize the information. A control code that follows certain rules is arranged, and these rules are implemented in the postprocessor. Generally, this process is relatively fixed and

uncomplicated. For the type of controller in the hybrid robot, a block of the control code at a dwell point i is set as (X_i, Y_i, Z_i, A_i, B_i, C_i, F_i). The first three items indicate the position of the variables of the three prismatic joints in the parallel robot. The next two items represent the variables of the two revolute joints in the serial robot. C_i denotes the variable of redundant rotation, and F_i represents the corresponding feed rate.

Finally, the process of robot control code generation is summarized using the flow chart in Fig. 9. Based on the process, a programming toolkit that can minimize the programming effort is developed using MATLAB. The tool path and control codes can be automatically processed and generated using the programming toolkit.

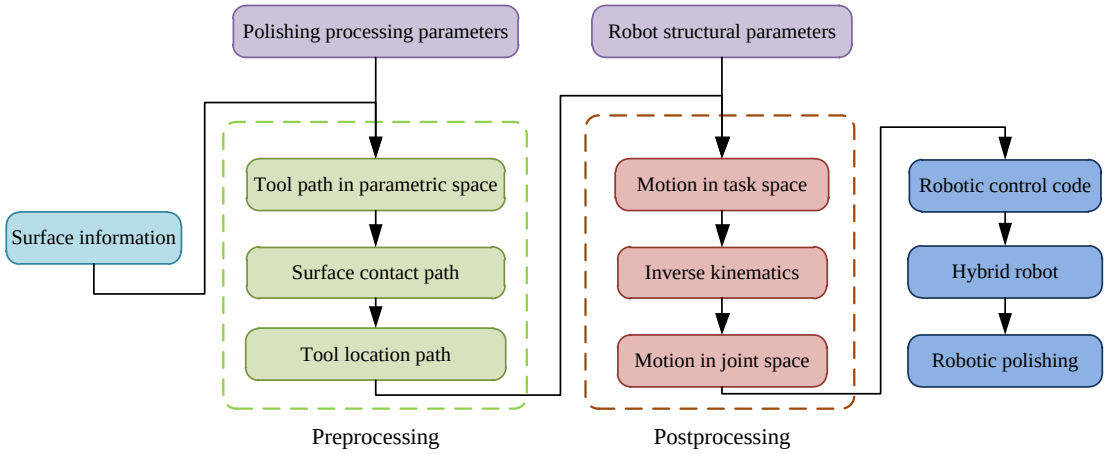

Fig. 9 Flow chart of the control code generation process.

4 Illustrative example

An experiment was conducted with a true freeform surface to verify the feasibility of the developed robot and the proposed control process. The robot control code file was generated, and a freeform polishing experiment was performed on the developed hybrid robot.

4.1 Robot control code generation

A bicubic Bézier surface, as a representative of the freeform surface, with an area of 40 mm × 40 mm was selected. Fig. 10 shows the oblique view and top view of the freeform surface. The polishing quality is affected by many parameters. In this example, the radius of the polishing tool

R_b was 10 mm, the inclination ρ was 15°, the compression amount of the tool d was 0.2 mm, and the attitude angle of the polishing tool ϕ was 0° or 180°.

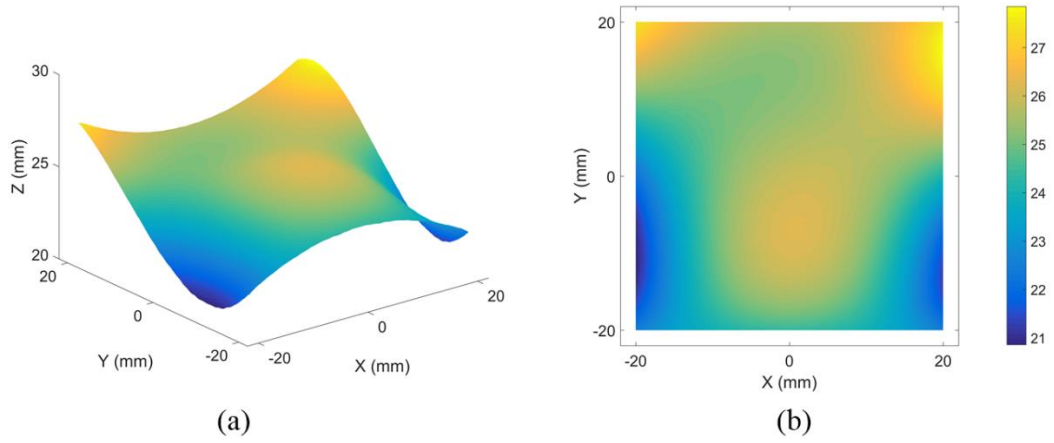

Fig. 10 Freeform surface: (a) oblique view, and (b) top view.

As shown in Fig. 11, the Hilbert curve in the 2D space was modified using circular arc transitions. To decrease the step length, points on each line segment were further densified. Using the mapping strategy, dwell points on the freeform surface were obtained. Meanwhile, the local normal vector at each dwell point on the freeform surface was also calculated. As shown in Fig. 12, a TCP path was attained by offsetting the surface path along the corresponding local normal directions. By comparing the surface path and the TCP path, it can be found that the top view of the surface path did not completely coincide with the TCP path because the local normal varies along the tool path. The deviations depend on the variations in curvature of the freeform surface. For a clear presentation, the path was illustrated with only the fourth-order Hilbert curve. A practical polishing path requires the TCP path to be calculated according to a group of optimized process parameters.

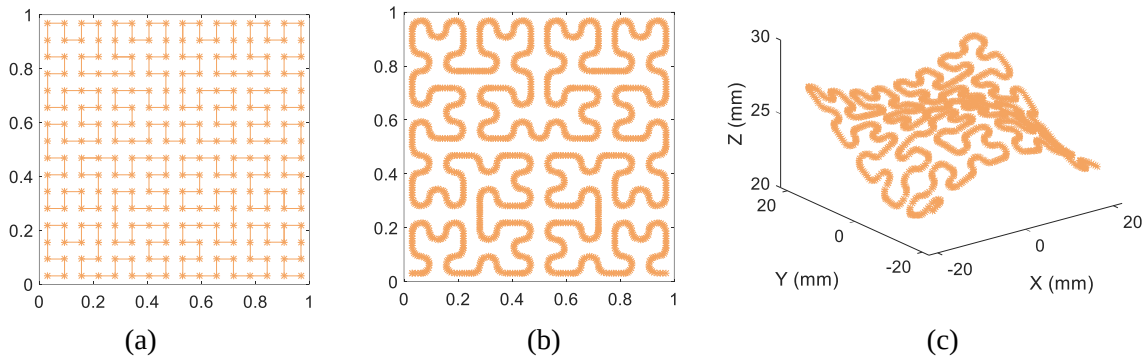

Fig. 11 Surface path generation on the freeform surface: (a) Hilbert curve, (b) parametric space, and (c) Cartesian space.

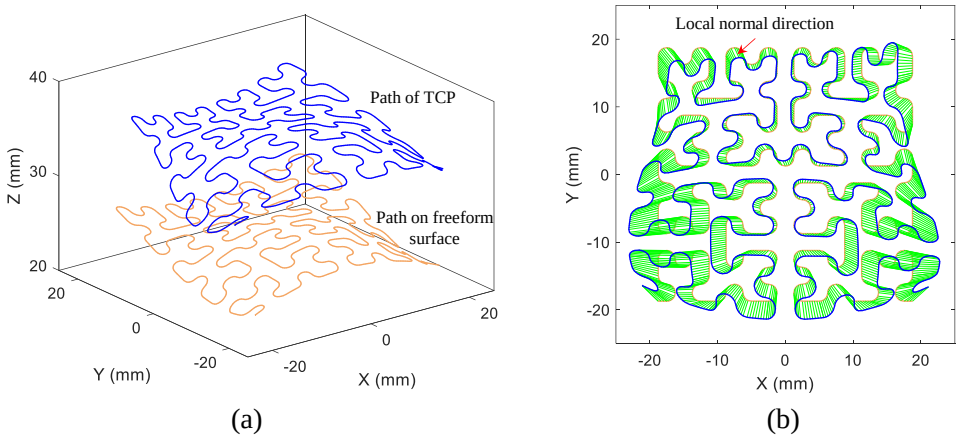

Fig. 12 Tool-path generation on the freeform surface.

Freeform polishing requires only five DOFs, where three are used for positioning, and two are used for orientating the tool axis. Therefore, the hybrid robot will generate one redundant DOF when it is used to perform freeform polishing. For convenience, θ_3 is considered as the redundant variable and is set to zero. For a given TCP path in the task space, the joint variables in the joint space can be calculated after postprocessing, as illustrated in Fig. 13. The final step involves converting these joint variables into an executable file format which can be received directly by the robot controller. Once the control code is generated, it is downloaded to the robot controller. After verification of the control code by trial polishing, it can be employed by the hybrid robot to conduct the polishing experiment.

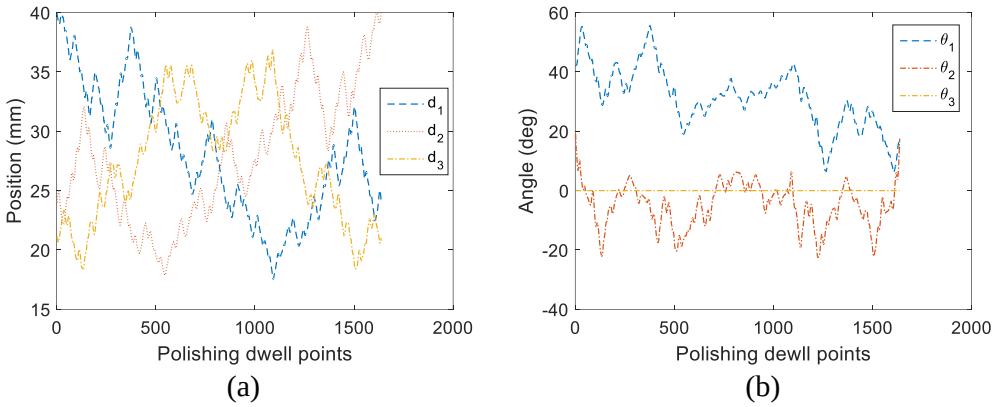

Fig. 13 Joint variables of the hybrid robot: (a) joint variables of the prismatic joints, and (b) joint variables of the revolute joints.

4.2 Experimental verification

Polishing experiments were performed to verify the developed process. As shown in Fig. 14, a 3D model of a workpiece with the surface illustrated in Fig. 10 was designed. A sample of the workpiece was fabricated using stainless steel and a common 3-axis machine tool, and the sample was roughly polished with sandpaper.

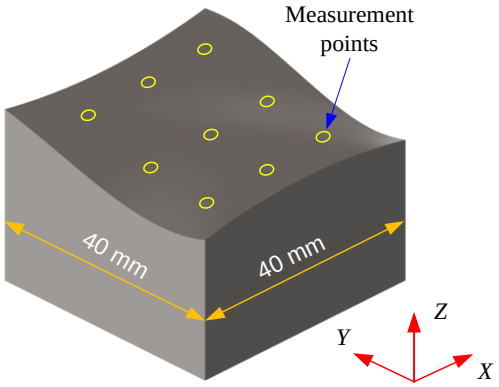

Fig. 14 3D-model of the workpiece with the freeform surface.

Fig. 15 demonstrates the polishing experiment of the freeform surface using the developed hybrid robot. The sample was clamped on the moving platform of the parallel robot with a collet. Several compliant polishing tools were fabricated using rubber with different elasticities and pad materials. The compliant tool was fixed on a steel shaft, allowing it to be mounted on the spindle of

the serial robot. The polishing force can be ensured using the compliant polishing tool. Currently, the geometrical errors of the hybrid robot are relatively high to achieve stable material influence for the corrective polishing mode. Fortunately, such errors can be avoided by the compliance of the tool in the pre-polishing step. Diamond compounds with different grades of abrasives were used during the polishing process. The polishing experiment was repeated four times with four different grades of abrasives (10 μm, 6 μm, 2 μm, and 1 μm). Each time, before executing the processing programs, the surface roughness values were measured off-line using a Zygo Nexview white light interferometer; the measuring points are given in Fig. 14. The spindle speed was set at 2000 rpm, and the used feed rate was 120 mm/min.

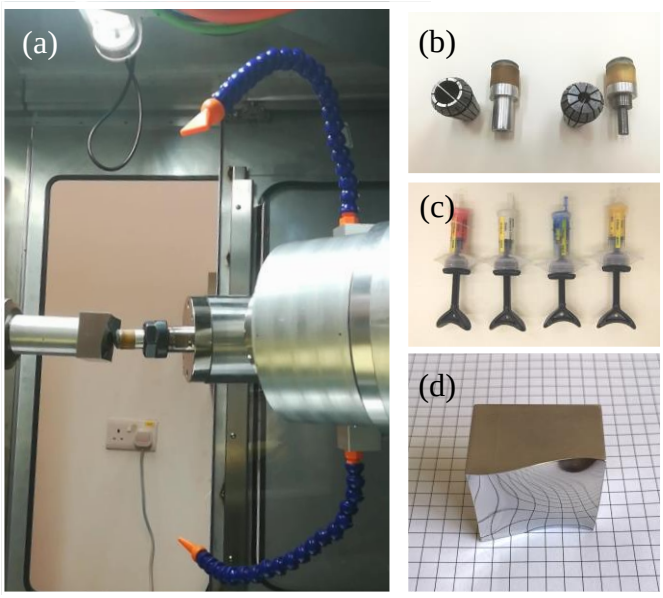

Fig. 15 Polishing experiment of the freeform surface: (a) polishing set-up; (b) polishing tool and collets, (c) diamond compound, and (d) freeform surface polishing result.

The pre-polishing experiment showed that the tool can move on the surface according to the desired motion specified by the control code, which indicates the feasibility of the hybrid robot and the programming toolkit. After polishing, a reflective mirror surface was obtained on the freeform surface. Fig. 16 shows the relationship between the surface roughness and the polishing cycles. A significant reduction in the surface roughness was observed after the first polishing cycle. As the number of polishing cycles increased, the surface roughness gradually converged to a threshold

value. The results also indicate that the surface roughness of each measurement point was relatively close, which means that the uniformity of the surface was improved.

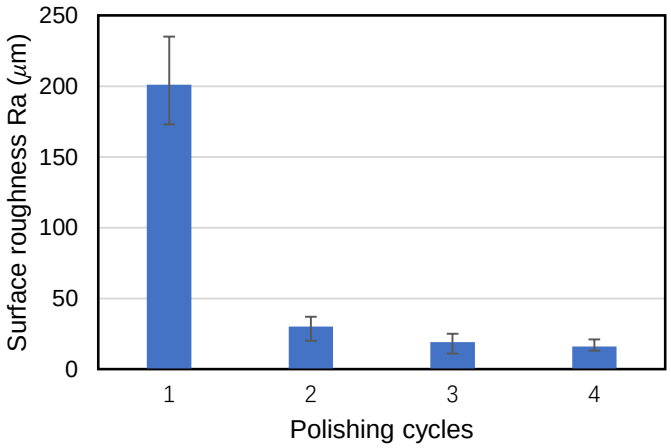

Fig. 16 Surface roughness in different polishing cycles.

Fig. 17 shows the surface texture and surface profile before and after polishing. The final surface roughness decreased from 201 nm to approximately 11 nm. The effective reduction in surface roughness confirms that the presented hybrid robot and the proposed control process are suitable for freeform polishing.

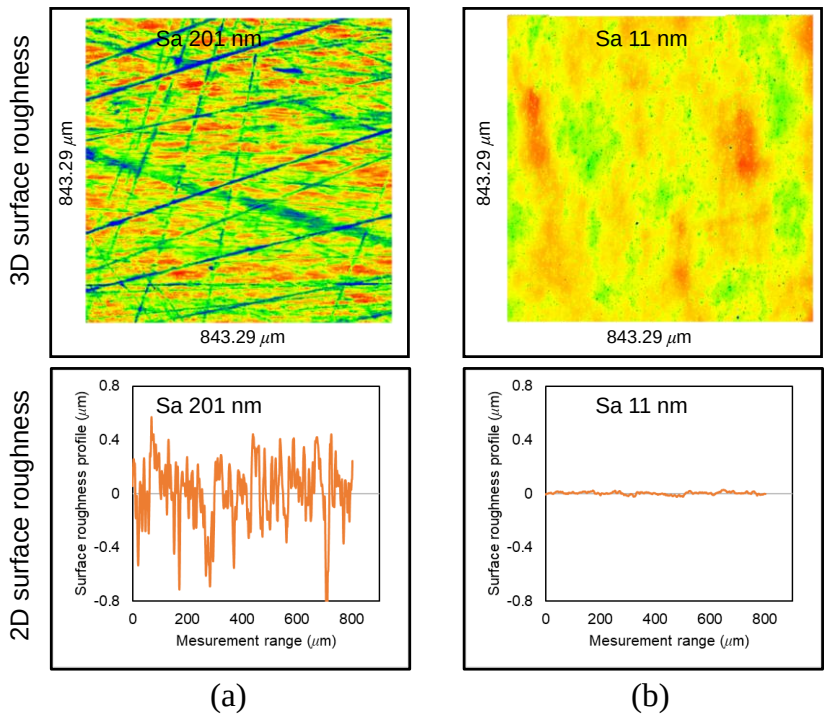

Fig. 17 Surface roughness of the freeform surface: (a) before polishing, and (b) after polishing.

5 Conclusions

In this study, we developed a novel custom-built hybrid robot with a smaller moving mass and a larger strength-to-weight ratio than those of conventional CNC machines. A control process that can realize automated freeform polishing with the hybrid robot was proposed. According to the desired polishing process parameters, an algorithm to generate random tool paths on freeform surfaces was developed to suppress repetitive patterns on polished surfaces. By offsetting the surface dwell points along the local normal direction, the TCP path could be generated in the workpiece frame. A dedicated postprocessor for the hybrid robot was developed based on the structural parameters and the kinematics model. The tool-path data were then converted into the control code that can be executed by the robotic controller. According to the process flow, a specially designed programming toolkit was developed corresponding to the hybrid robot. The toolkit can help the operator directly generate control codes that conform to the developed hybrid robot.

A freeform stainless-steel surface was polished using the developed hybrid robot. The effectiveness of the hybrid robot and the control process were confirmed as the tool could move

according to the desired tool path. The polishing results indicated that a reflective mirror surface was obtained on the freeform surface, and the measurement results showed that the surface roughness was significantly reduced from 201 nm to 11 nm, which further demonstrates the effectiveness of the hybrid robot and the presented control process.

Acknowledgments

The authors would also like to express their sincere thanks to the Innovation and Technology Commission (ITC) of the Government of the Hong Kong Special Administrative Region (HKSAR) for the financial support under the Projects no. GHP/031/13SZ.

References

[1] Cheung CF, Kong LB, Ho LT, To S. Modelling and simulation of structure surface generation using computer controlled ultra-precision polishing. Precis Eng 2011;35:574-90.

[2] Pessoles X, Tournier C. Automatic polishing process of plastic injection molds on a 5-axis milling center. J Mater Process Tech 2009;209:3665-73.

[3] Chaves-Jacob J, Linares J, Sprauel J. Control of the contact force in a pre-polishing operation of free-form surfaces realised with a 5-axis CNC machine. CIRP Annals 2015;64:309-12.

[4] Fan C, Hong GS, Zhao J, Zhang L, Zhao J, Sun L. The integral sliding mode control of a pneumatic force servo for the polishing process. Precis Eng 2019;55:154-70.

[5] Guo J, Suzuki H, Morita S-y, Yamagata Y, Higuchi T. A real-time polishing force control system for ultraprecision finishing of micro-optics. Precis Eng 2013;37:787-92.

[6] Jin M, Ji S, Pan Y, Ao H, Han S. Effect of downward depth and inflation pressure on contact force of gasbag polishing. Precis Eng 2017;47:81-9.

[7] Mohammad A, Hong J, Wang DW. Design of a force-controlled end-effector with low-inertia effect for robotic polishing using macro-mini robot approach. Robot Comput Integr Manuf 2018;49:54-65.

[8] Solanes JE, Gracia L, Muñoz-Benavent P, Miro JV, Perez-Vidal C, Tornero J. Robust hybrid position-force control for robotic surface polishing. J Manuf Sci Eng 2019;141:011013.

[9] Wan S, Zhang X, Wang W, Xu M, Jiang X. Edge control in precision robotic polishing based on space-variant deconvolution. Precis Eng 2019;55:110-8.

[10] Guo J, Liu K, Wang Z, Tnay GL. Magnetic field-assisted finishing of a mold insert with curved

microstructures for injection molding of microfluidic chips. Tribol Int 2017;114:306-14.

[11] Walker D, Dunn C, Yu G, Bibby M, Zheng X, Wu HY, et al. The role of robotics in computer controlled polishing of large and small optics. In: Procceding of SPIE optical manufacturing and testing; 2015, p. 1-9.

[12] Liao L, Xi FF, Liu KF. Modeling and control of automated polishing/deburring process using a dual-purpose compliant toolhead. Int J Mach Tool Manu 2008;48:1454-63.

[13] Chong Z, Xie F, Liu X-J, Wang J, Niu H. Design of the parallel mechanism for a hybrid mobile robot in wind turbine blades polishing. Robot Comput Integr Manuf 2020;61.

[14] Huang T, Zhao D, Cao Z-C. Trajectory planning of optical polishing based on optimized implementation of dwell time. Precis Eng 2020;62:223-31.

[15] Lai Y-L, Liao C-C, Chao Z-G. Inverse kinematics for a novel hybrid parallel–serial five-axis machine tool. Robot Comput Integr Manuf 2018;50:63-79.

[16] Wang D, Wu J, Wang L, Liu Y. A post-processing strategy of a 3-DOF parallel tool head based on velocity control and coarse interpolation. IEEE T Ind Electron 2017;65:6333-42.

[17] Cao ZC, Cheung CF, Zhao X. A theoretical and experimental investigation of material removal characteristics and surface generation in bonnet polishing. Wear 2016;360:137-46.

[18] Cheung CF, Ho LT, Charlton P, Kong LB, To S, Lee WB. Analysis of surface generation in the ultraprecision polishing of freeform surfaces. P I Mech Eng B-J Eng 2010;224:59-73.

[19] Dunn CR, Walker DD. Pseudo-random tool paths for CNC sub-aperture polishing and other applications. Opt Express 2008;16:18942-9.

[20] Wang CJ, Wang ZZ, Xu Q. Unicursal random maze tool path for computer-controlled optical surfacing. Appl Optics 2015;54:10128-36.

[21] Takizawa K, Beaucamp A. Comparison of tool feed influence in CNC polishing between a novel circular-random path and other pseudo-random paths. Opt Express 2017;25:22411-24.

[22] Dong ZC, Nai WZ. Surface ripple suppression in subaperture polishing with fragment-type tool paths. Appl Optics 2018;57:5523-32.

[23] Tam HY, Cheng HB. An investigation of the effects of the tool path on the removal of material in polishing. J Mater Process Tech 2010;210:807-18.

[24] Lin FY, Lu TS. Development of a robot system for complex surfaces polishing based on CL data. Int J Adv Manuf Technol 2004;26:1132-7.

[25] Chen S-L, Chang T-H, Inasaki I, Liu Y-C. Post-processor development of a hybrid TRR-XY parallel kinematic machine tool. Int J Adv Manuf Technol 2002;20:259-69.

[26] Gosselin C, Angeles J. A Global Performance index for the kinematic optimization of robotic manipulators. J Mech Design 1991;113:220-6.

[27] Nirala HK, Agrawal A. Fractal geometry rooted incremental toolpath for incremental sheet forming. J Manuf Sci Eng 2017;140.

[28] Shaikh S, Kumar N, Jain PK, Tandon P. Hilbert curve based toolpath for FDM process. CAD/CAM, Robotics and Factories of the Future: Springer, 2016. p. 751-9.

[29] Wang C, Cheung C, Xu P, Li B, Ho L. Research on computer controlled ultra-precision polishing of freeform surfaces. In: Procceding of SPIE optical precision manufacturing, testing, and applications; 2018, p. 1-8.

[30] Cao ZC, Cheung CF, Liu MY. Model-based self-optimization method for form correction in the computer controlled bonnet polishing of optical freeform surfaces. Opt Express 2018;26:2065-78.

[31] Choi YK, Banerjee A, Lee JW. Tool path generation for free form surfaces using Bezier curves/surfaces. Comput Ind Eng 2007;52:486-501.

[32] Tam HY, Cheng H, Dong Z. Peano-like paths for subaperture polishing of optical aspherical surfaces. Appl Opt 2013;52:3624-36.

[33] Dong J, Yu T, Chen H, Li B. An improved calculation method for cutting contact point and tool orientation analysis according to the CC points. Precis Eng 2020;61:1-13.

[34] Xu P, Cheung C-F, Li B, Ho L-T, Zhang J-F. Kinematics analysis of a hybrid manipulator for computer controlled ultra-precision freeform polishing. Robot Comput Integr Manuf 2017;44:44-56.

[35] Wang C, Wang Z, Wang Q, Ke X, Zhong B, Guo Y, et al. Improved semirigid bonnet tool for high-efficiency polishing on large aspheric optics. Int J Adv Manuf Technol 2016;88:1607-17.